Oxygen induced effects on avascular tumour growth: a preliminary simulation using an adaptive grid algorithm

2015 J. Phys.: Conf. Ser. 633 012088

(http://iopscience.iop.org/1742-6596/633/1/012088)

Journal of Physics: Conference Series **633** (2015) 012088 doi:10.1088/1742-6596/633/1/012088

Oxygen induced effects on avascular tumour growth: a preliminary simulation using an adaptive grid algorithm

Antonino Amoddeo

Department of Civil, Energy, Environmental and Materials Engineering, Università 'Mediterranea' di Reggio Calabria,Via Graziella 1, Feo di Vito, I-89122 Reggio Calabria, Italy

E-mail: antonino.amoddeo@unirc.it

Abstract. Cancer cells oxygenation from surrounding healthy tissue influences tumour growth in the avascular phase. The effects induced by oxygen on cancer cells dynamics during their interaction with the urokinase plasminogen activator system, are simulated mimicking hypoxic conditions in the early stage of human tumour proliferation, using oxygen supply parameters determined from *in vivo* experiments. The system of six coupled partial differential equations, arising from the problem modelling, is solved over a one-dimensional domain implementing a moving mesh numerical technique, using the finite element method. Our preliminary computations show that oxygen concentration at hypoxic conditions cause cancer cells to build inhomogeneous proliferation pattern, similarly to what happens in absence of oxygen.

1. Introduction

Cancer cells dynamics is the result of the interaction among several biological mechanisms, covering phenomena occurring over different length scales [1]. On one hand it is relatively easy to obtain data on avascular tumour growth from *in vitro* experiments performed on multicellular spheroids, on the other cannot be ignored that during *in vivo* proliferation, microenvironment mechanisms occur, not present in *in vitro* experiments [2]. The presence of oxygen in cancer tissue, coming from the surrounding healthy tissue, can influence the sensitivity of the cells to, for example, nonsurgical treatments as radiotherapy, and most of malignancies are characterized by the heterogeneous presence of hypoxic tissue areas [3]. The deadly stage of tumour proliferation begins when the sprout of new blood vessels allows cancer cells to reach region of healthy tissue, or organs, located far from the initial tumour mass, sowing with metastasis [4]. Reviews about modelling of cancer cell growth and proliferation can be found, among others, in references [5-7].

Models of tumour growth inside biological tissue are expressed as systems of partial differential equations (PDEs) [8], considering an initial cluster of cancer cells seeded in the extracellular matrix (ECM), a nutrient-rich aqueous environment allowing the cells to grow and proliferate [1]. A mechanism recognized as promoting cancer cell growth and proliferation is their interaction with the urokinase plasminogen activator (uPA) system: in short, the uPA serine protease degrades an ECM macromolecule, vitronectin (VN), while the ECM enzyme plasmin activates uPA; the plasminogen activator inhibitor type-1 (PAI-1) secreted by healthy cells regulates excess of proteolysis, see [9] for details about biological foundations and descriptions.

The above mechanism has been recently simulated over a one-dimensional domain, and the PDEs system arising from the problem modelling has been solved implementing the moving mesh partial differential equation (MMPDE) numerical technique [10], using the finite element method (FEM) [11]. As elsewhere shown and discussed [12-15], in such technique the discretization of the integration domain, typical of the FEM procedure, is controlled by the gradient of a parameter calculated during the solution procedure, in our case the gradient of the cancer cells concentration [10], using the equidistribution principle [16]: it results a non-uniform node distribution, but nodal connectivity and number of mesh points inside the integration domain are kept constant, while the mesh points are moved in regions where more detail is required.

We present a preliminary simulation of the tumour progression in a one-dimensional portion of biological tissue, in the early stage of the avascular phase under hypoxic conditions. The PDEs system which arises modelling the interaction of cancer cells dynamics with both the uPA system and a model for oxygen supply is solved using the MMPDE numerical technique. The method results appropriate in presence of rapidly varying parameters, as in shocks or defects, leading to sharp solution features [12-15], allowing to capture finer spatial details related to malignancy.

2. Theory and method

We assume that cell migration inside a given biological domain originates from random diffusion, chemotaxis and haptotaxis: in particular, chemotaxis is the cell movement towards chemicals dissolved in the ECM, while haptotaxis is the attraction of the cells by chemicals adhered to some ECM component [10].

In a fixed domain $\Omega \subset \mathbb{R}^3$, we consider explicitly the concentration evolution of cancer cell, VN protein, uPA serine protease, PAI-1 inhibitor, plasmin degrading enzyme and oxygen concentration, denoted, respectively, by $c(\mathbf{x},t)$, $v(\mathbf{x},t)$, $u(\mathbf{x},t)$, $p(\mathbf{x},t)$, $m(\mathbf{x},t)$ and $n(\mathbf{x},t)$, according to the following system of coupled PDEs:

$$\frac{\partial c}{\partial t} = \nabla \cdot \left[D_c \nabla c - c\left(\chi_u \nabla u + \chi_p \nabla p + \chi_v \nabla v \right) \right] + \mu_1 c\left(1 - c\right) + k_2 nc \tag{1}$$

$$\frac{\partial v}{\partial t} = -\delta v m + \phi_{21} up - \phi_{22} vp + \mu_2 v\left(1 - v\right) \tag{2}$$

$$\frac{\partial u}{\partial t} = \nabla \cdot \left(D_u \nabla u \right) - \phi_{31} pu - \phi_{33} cu + \alpha_{31} c \tag{3}$$

$$\frac{\partial p}{\partial t} = \nabla \cdot \left(D_p \nabla p \right) - \phi_{41} pu - \phi_{42} pv + \alpha_{41} m \tag{4}$$

$$\frac{\partial m}{\partial t} = \nabla \cdot \left(D_m \nabla m \right) + \phi_{52} pv + \phi_{53} cu - \phi_{54} m \tag{5}$$

$$\frac{\partial n}{\partial t} = \nabla \cdot \left(D_n \nabla n \right) + k_1 n_0 (1 - c) - k_1 n - k_2 nc \tag{6}$$

In equation (1), the migration of cancer cells is accounted for by random motility, chemotaxis due to the presence of both uPA and PAI-1 molecules, and haptotaxis due to VN, via, respectively, D_c, χ_u, χ_p, and χ_v; cells production term includes contributions from logistic growth at a rate μ_1, and from oxygen interaction through k_2. Vitronectin cannot diffuse: it is degraded by plasmin at a rate δ, indirectly produced from the interaction of PAI-1 with uPA at a rate ϕ_{21}, neutralized by PAI-1 inhibitor at a rate ϕ_{22}, and produced according to cell proliferation at a rate μ_2, see equation (2). Concerning equation (3), uPA diffuses at a rate D_u and is inhibited by PAI-1 at a rate ϕ_{31}; cancer cells cause its degradation at a rate ϕ_{33} through their mutual interaction, and its production at a rate α_{31}. In equation (4), PAI-1

inhibitor diffuses at a rate D_p, the interactions with uPA and VN degrade it at a rate of, respectively, ϕ_{41} and ϕ_{42}, while it is produced by plasmin at a rate α_{41}. Considering plasmin, equation (5), it moves according to D_m, is produced by both PAI-1 binding to VN and uPA binding to cancer cells at a rate, respectively, ϕ_{52} and ϕ_{53}, and degrades at a rate ϕ_{54}. Finally, let n_0 be the initial concentration of oxygen in absence of cancer cells, assuming its utilization from cancer cells only, it diffuses according to D_n, degrades at a rate k_1, while it is utilized by cancer cells at a rate k_2, equation (6).

The coupled equations (1) - (6) constitute a PDEs system, which solution starts from the discretization of the one dimensional integration domain, equidistributing in each subinterval a monitor function depending on the gradient of the unknown solution. Denoting as $\Omega_p = [0,1]$ and $\Omega_c = [0,1]$, respectively, physical and computational domains, $u(z,t)$ a solution of a PDEs system over Ω_p with z physical coordinate, and ξ a computational coordinate of a fixed computational domain, a one-to-one mapping from physical space $\Omega_p \times (0,T]$ to computational space $\Omega_c \times (0,T]$ is defined as $\xi = \xi(z,t)$, $z \in \Omega_p$, $t \in (0,T]$, while $z = z(\xi,t)$, $\xi \in \Omega_c$, $t \in (0,T]$ is from computational space $\Omega_c \times (0,T]$ to physical space $\Omega_p \times (0,T]$. From the equidistribution of a monitor function $M(u(z,t))$ over our one-dimensional domain we obtain the mesh equation

$$M(z(\xi,t))\frac{\partial}{\partial \xi} z(\xi,t) = \int_0^1 M(u(s,t))\,ds = C(t), \tag{7}$$

and the choice of the monitor function tested by Beckett et al. [17], ensures a good quality control of the node distribution and final convergence of the FEM solution, with the additional advantages of being naturally smoothed, and not demanding external interventions, then

$$M(u(z,t)) = \int_0^1 \left(\left|\frac{\partial u(z,t)}{\partial z}\right|\right)^{1/2} dz + \left(\left|\frac{\partial u(z,t)}{\partial z}\right|\right)^{1/2}. \tag{8}$$

The adaptive solution involves an iterative process in which, at each time step, (i) a mesh is generated using the equidistribution principle based on the numerical solution at the current time step and (ii) the PDEs is solved on a new generated grid and the solution is updated in time.The one-dimensional domain is initially discretized via the method of lines, using an implicit Euler method for time discretization. See [12-15] for details about the MMPDE procedure. We used dimensionless quantities obtained by scaling all variables and parameters by reference quantities: distance x is scaled with the maximum distance for cancer cells $L = 10^{-1}$ cm; let $D = 1 \times 10^{-6}$ cm^{2}s^{-1} be a representative diffusion coefficient, time t is scaled according to $\tau = L^2D^{-1}$. A reference cancer cell concentration is $c_0 = 6.7 \times 10^7$ cell cm^{-3}, while uPA, VN, PAI-1 and plasmin, are scaled according to appropriate reference concentration values, $u_0 = 1$ nM, $v_0 = 1$ nM, $p_0 = 1$ nM, $m_0 = 0.1$ nM, respectively [9]. Furthermore, $D_c = 3.5 \times 10^{-4}$, $D_u = 2.5 \times 10^{-3}$, $D_p = 3.5 \times 10^{-3}$, $D_m = 4.91 \times 10^{-3}$, $\chi_u = 3.05 \times 10^{-2}$, $\chi_p = 3.75 \times 10^{-2}$, $\chi_v = 2.85 \times 10^{-2}$, $\mu_1 = 0.25$, $\mu_2 = 0.15$, $\alpha_{31} = 0.215$, $\alpha_{41} = 0.5$, $\delta = 8.15$, $\phi_{21} = 0.75$, $\phi_{22} = 0.55$, $\phi_{31} = 0.75$, $\phi_{33} = 0.3$, $\phi_{41} = 0.75$, $\phi_{42} = 0.55$, $\phi_{52} = 0.11$, $\phi_{53} = 0.75$, $\phi_{54} = 0.5$.

Concerning oxygen, its diffusion coefficient has been estimated in various biological environment in the 1.3×10^{-5} cm^{2}s^{-1} ÷ 3.1×10^{-5} cm^{2}s^{-1} range [18], hence, we put $D_n = 25$; the others model parameters come from *in vivo* measurements on human tumours, and to mimic hypoxic conditions typical of malignant proliferations [3] we put $k_2 = 0.3$, $n_0 = 1.37$ μM, serving also as reference concentration, while we assume $k_1 = 0.5 \times k_2 = 0.15$ [8]. We impose that at $t = x = 0$, a cluster of cancer cells is seeded in the domain, while the remaining portion of tissue is filled by ECM; moreover, the initial concentrations of uPA and PAI-1 are proportional to the cancer cells concentration, plasmin is not yet produced, and the oxygen concentration is at the initial concentration. Therefore, $c(\mathbf{x},0) = \exp(-|\mathbf{x}|^2\varepsilon^{-1})$ with $\varepsilon = 0.01$, $v(\mathbf{x},0) = 1 - 0.5c(\mathbf{x},0)$, $u(\mathbf{x},0) = 0.5c(\mathbf{x},0)$, $p(\mathbf{x},0) = 0.05c(\mathbf{x},0)$, $m(\mathbf{x},0) = 0$ [13,14] and $n(\mathbf{x},0) = n_0$. The components cannot break-out from the simulated domain, then zero-flux boundary conditions have been imposed on our PDEs system, apart from the ordinary differential equation (2). We show the numerical simulation over a one dimensional portion of biological tissue 2 mm thick,

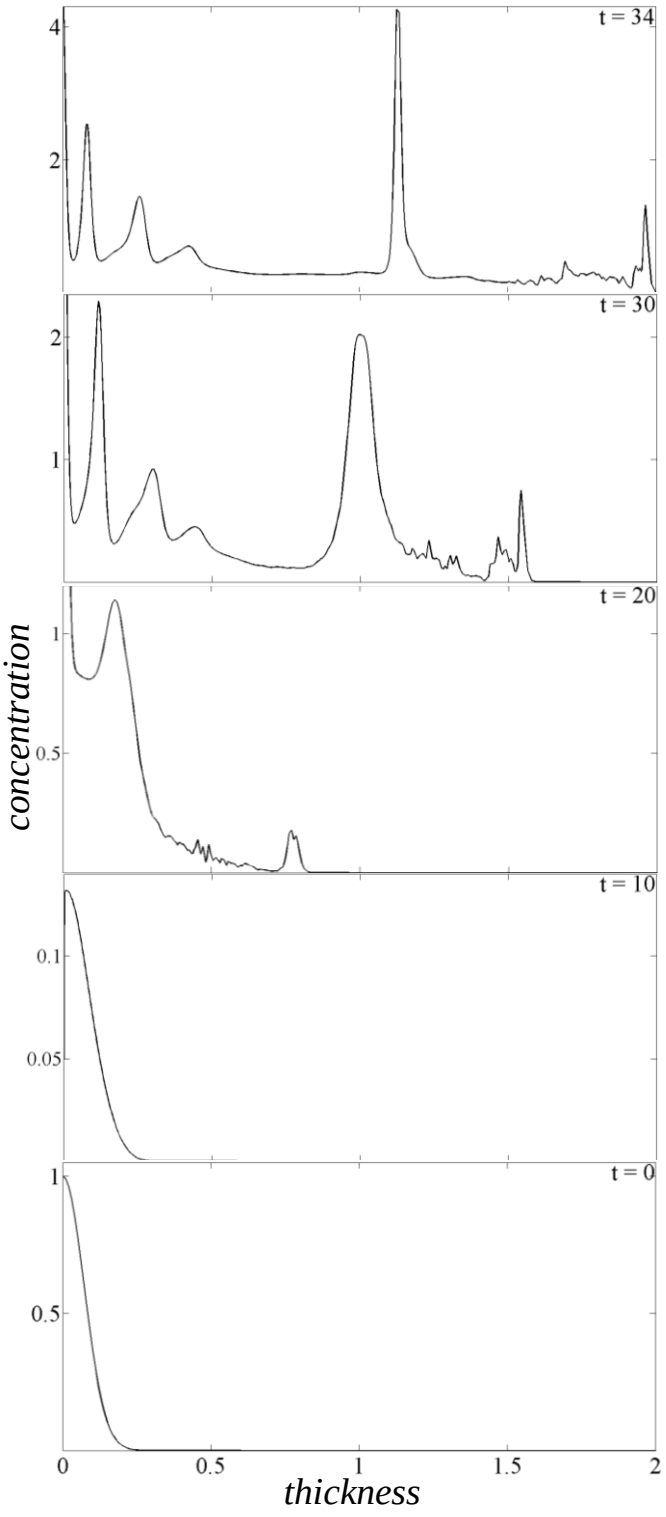

Figure 1. Concentration evolution of cancer cells *c* along the tissue thickness. Each panel corresponds to a snapshot taken during the time evolution.

with 200 grid points, for $x \in [0,2]$, $t \in [0,100]$ and steps δt=0.5. Both the dimensional thickness and timescale are recovered multiplying, respectively, *x* by *L* and *t* by τ. At each time step our PDEs system has been solved replacing the exact solution *u(x,t)* in equation (8), with *c(x,t)*.

3. Results and discussion

In figure 1 we show snapshots of the cancer cells density profile taken at selected times during the proliferation process: horizontal and vertical axes report, respectively, the tissue thickness in the $0 \leq x \leq 2$ range and the cancer cell concentration. At t=0 the density profile reflects the initial conditions, and until t=10 the cells remains clustered around x=0. At t=20 it appears radically changed: the invasion front moves near x=1; a sharp onset marks the cancer/healthy cells interface, coming with an irregular and jagged fine structure. For t=30 the invading front is beyond x=1.5, while, at t=34, it reaches x=2.

In a continuum frame, the whole set of density profiles builds the spatio-temporal proliferation pattern shown in figure 2, where the cancer cells density is linearly mapped in a grey level scale between black and white colours, respectively zero and maximum density. On the vertical axis the time scale of the solution evolution is in the $0 \leq t \leq 100$ interval. The interaction between uPA system and cancer cells, in presence of oxygen in the micromolar range, gives rise to marked inhomogeneity of the spatio-temporal proliferation: such behaviour is consistent to what recently observed in absence of oxygen [10], and evidence of malignancy [5].

4. Conclusions

We have presented a preliminary numerical simulation of the effects induced by oxygen during the interaction of uPA system with cancer cell dynamics. The results indicate malignant proliferation through heterogeneous spatio-temporal patterns, in continuity with our previous modelling performed in

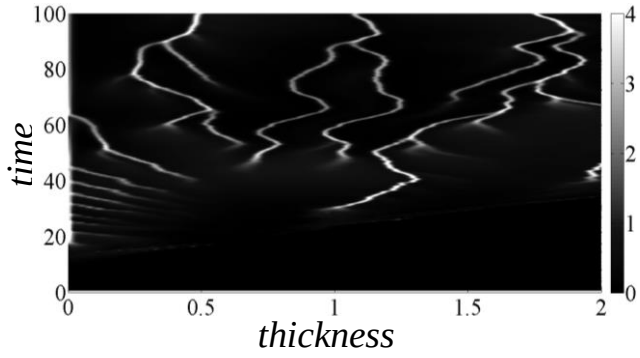

Figure 2. Surface contour plots of the cancer cells evolution in the $0 \leq x \leq 2$ spatial domain and in the $0 \leq t \leq 100$ time interval. The cell concentration is linearly mapped in a grey levels scale between the black (zero concentration) and white (maximum concentration) colours.

absence of oxygen. The peculiarity of the MMPDE technique relies on the cell density-driven mechanism used to discretize the integration domain, letting the grid points to cluster in region where ∇c is growing, and allowing to resolve the fine structure coming with the irregular invading front at the boundary between cancer ad healthy cells. It results, with respect to techniques based on uniform discretizations, an improved resolution of features related to the heterogeneous spatial distribution of malignant cells.

References

[1] Preziosi L and Tosin AR 2009 *J. Math. Biol.* **58** 625-56
[2] Sherratt JA and Chaplain MAJ 2001 J. *Math. Biol.* **43** 291-312
[3] Vaupel P, Kallinowski F and Okunieff P 1989 *Cancer Research* **49** 6449-65
[4] Chaplain MAJ and Anderson ARA 2003 Mathematical modelling of tissue invasion *Cancer Modelling and Simulation* ed L Preziosi (Boca Raton: Chapman & Hall/CRC Press) p. 269
[5] Araujo RP and McElwain DLS 2004 *Bull. Math. Biol.* **66** 1039-91
[6] Roose T, Chapman SJ and Maini PK 2007 *SIAM Rev.* **49** 179-208
[7] Lowengrub JS, Frieboes HB, Jin F, Chuang YL, Li X, Macklin P, Wise SM and Cristini V 2010 *Nonlinearity* **23** R1-R91
[8] Hubbard ME and Byrne HM 2013 *J. Theor. Biol.* **316** 70-89
[9] Andasari V, Gerisch A, Lolas G, South AP and Chaplain MAJ 2011 *J. Math. Biol.* **63** 141-71
[10] Amoddeo A 2015 *Comput. Math. Appl.* (in press).
[11] Zienkiewicz OC and Taylor RL 2002 *The Finite Element Method* (Oxford: Butterworth–Heinemann)
[12] Amoddeo A, Barberi R and Lombardo G 2010 *Comput. Math. Appl.* **60** 2239-52
[13] Amoddeo A, Barberi R and Lombardo G 2011 *Liq. Cryst.* **38** 93-103
[14] Amoddeo A, Barberi R and Lombardo G 2012 *Phys. Rev.* E **85** 061705-10
[15] Amoddeo A, Barberi R and Lombardo G 2013 *Liq Cryst.* **40** 799-809
[16] de Boor C 1974 Good approximation by splines with variable knots II *Lecture Notes in Mathematics* vol 263, ed J Morris (Berlin: Springer-Verlag) pp 12-20
[17] Beckett G, Mackenzie JA, Ramage A and Sloan DM 2001 *J. Comput. Phys.* **167** 372-92
[18] Buchwald P 2009 *Theor. Biol. Med. Model.* **6** 5